Overview of the Globus-M Spherical Tokamak Results

V.K.Gusev, B.B.Ayushin, F.V.Chernyshev, I.N.Chugunov, V.V.Dyachenko, L.A.Esipov, D.B.Gin, V.E.Golant, S.A. Khitrov, N.A.Khromov, S.V.Krikunov, G.S.Kurskiev, M.M.Larionov, R.G.Levin, V.B.Minaev, E.E.Mukhin, A.N.Novokhatskii, M.I.Patrov, Yu.V.Petrov, K.A.Podushnikova, V.V.Rozhdestvensky, N.V.Sakharov, O.N.Shcherbinin, A.E.Shevelev, S.Yu.Tolstyakov, V.I.Varfolomeev, M.I.Vildjunas, A.V.Voronin
Ioffe Physico-Technical Institute, RAS, 194021, St.-Petersburg, Russia
E-mail: vasily.gusev@mail.ioffe.ru
V.G.Kapralov , I.V.Miroshnikov, V.A.Rozhansky, I.Yu.Senichenkov, A.S.Smirnov, I.Yu.Veselova
St.-Petersburg State Polytechnical University, 195251, St.-Petersburg, Russia
S.E.Bender, V.A.Belyakov, Yu.A.Kostsov, A.B.Mineev, V.I.Vasiliev
D.V. Efremov Institute of Electrophysical Apparatus, 196641, St. Petersburg, Russia
E.A.Kuznetsov, V.N.Scherbitskii, V.A.Yagnov
SSC RF TRINITI, 142192, Moscow region, Russia
A.G.Barsukov, V.V.Kuznetsov, V.M.Leonov, A.A.Panasenkov, G.N.Tilinin
NFI RRC "Kurchatov Institute", 123182, Moscow, Russia
E.G.Zhilin
Ioffe Fusion Technology Ltd., 194021, St.-Petersburg, Russia

Abstract. A diminishing of impurities concentration in the discharge and the loop voltage decrease was achieved in the Globus-M spherical tokamak as a result of technological improvements. During experiments on density limit investigation in OH and NBI heating regimes the average density in 0.4T magnetic field was reached in excess of $1.1 \cdot 10^{20}$ m^{-3} with gas puff supply only. The role of core long wave MHD fluctuations and their coupling with peripherial modes is outlined. Greenwald limit was achieved. The NBI fast particles slowing down spectrum was measured and found to be in agreement with classical Coulomb scattering theory. During NBI low plasma density regimes with overheated ions and high density regimes with features of electron heating were obtained and studied. The fundamental harmonic ICR heating of hydrogen "minority" in deuterium plasma showed that the heating efficiency is relatively high and is improving with hydrogen concentration increase in the range of 10-70%. The role of the second harmonic is clarified. Plasma jet injection into Globus-M with a double-stage plasma gun showed that jet penetrated into the plasma as a time-of-flight recombined dense flux of neutrals. First numerical simulations of jet interaction with core plasma were done and showed that jet could penetrate beyond the separatrix. This doesn't contradict interferometric and local density measurements performed by Thomson scattering.

1. Introduction

Spherical tokamak Globus-M is aimed at investigation of a high beta low aspect ratio plasma (*R=0.36 m, a=0.24 m*) which is heated by up to 1 MW Neutral Beam Injection (NBI) and up to 0.4MW RF power in the ion cyclotron resonance (ICR) range at the current stage.

One of the most attractive fusion relevant scenarios is a high plasma density regime. Due to its unique technical characteristics, Globus-M has previously adopted the development of density control methods as one of its program goals. Designed B_T/R ratio is the highest among currently operating spherical tokamaks [1] and allows to increase current density and to "digest" high influx of neutrals, without shrinking of current channel and disruption.

NBI auxiliary heating, when used on small tokamaks has principal difficulties in realization due to small size of the target plasma compared to the beam dimensions and small size of the vacuum vessel compared to fast particle orbit extent. In ST's low magnetic field complicates the problem of fast ion confinement, moreover in Globus-M plasma is tightly fitted into the vacuum vessel.

A significant part of Globus-M research activities is connected with ICR plasma heating at fundamental harmonic frequency. Unlike conventional tokamaks, in spherical tokamaks simultaneous existence of several IC harmonics in the plasma cross-section take place, in which RF power absorption is possible with different efficiency. Steep magnetic field gradient and low RF frequency decrease the width of resonance absorption layers and make them much smaller than excited wave length. Other specific features of this method are discussed in [2].

Development of density control methods alternative to gas puffing is an important task of researches performed at Globus-M. Experiments with injection of dense plasma jet with high velocity into the spherical tokamak Globus-M [3, 4, 5] have demonstrated the viability of such fuelling method with minimum plasma perturbations.

Further improvement of the device performance has been made since 20th IAEA FEC, 2004. In the target OH plasma discharges loop voltage was decreased down to 1 V. EFIT equilibrium reconstruction was improved and became a routine procedure with a data base of several thousands shots. Correction of central solenoid stray field and plasma column vertical and horizontal control improvement were made. A new system for a feedback control of the plasma current waveform and amplitude was commissioned. A diagnostics improvement has been made. The operating range of the microwave interferometer was enhanced by decreasing the probing wave length from 1.2 to 0.8 mm, which provided reliable density measurements. A new 32-channel SXR pinhole camera and a set of 44 in-vessel Mirnov coils provided MHD-mode identification [6]. The plasma density and temperature profiles were measured by multipulse Thomson scattering diagnostics. First measurements of the ion temperature made by new CHERS diagnostics are in agreement with NPA data. The present report is devoted to overview of results achieved on Globus-M in the field of activities referred above for the period.

2. High Density Experiments

Until recent experiments, however, various technical difficulties have prevented realizing the potential advantage of high B_T/R ratio in Globus-M. As usual on the route to high density regimes there are principal problems related to maintaining of plasma stability and peripheral power and particle balance. In our previous experiments [7] the highest densities obtained in OH regime in the non boronized vacuum vessel were below 4×10^{19} m^{-3}. The boronization allowed us to increase the limit up to $(5\text{-}6)\times10^{19}$ m^{-3} which corresponded to the value of ~0.75 n_{Gr}. At the densities higher than 5×10^{19} m^{-3} strong MHD instability of coupled 1/1 and 2/1 tearing modes developed, this restricted further density rise. Typical behavior of such instability is shown in Fig.1. Both modes have common frequency that evidences of their toroidal coupling. Locking of the modes leads to an internal reconnection event (IRE), manifesting itself in a characteristic spike on the plasma current trace. During the experimental campaign described in [8] we increased essentially the density limit due to several steps. First, we have eliminated most of vertical displacement instabilities by improvement of the plasma column vertical position sensor and controller. Second, permanent improvement in the vessel

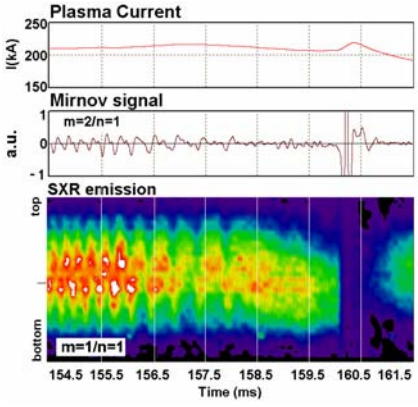

Fig.1 *Locking of 2/1 (Mirnov signal) and 1/1 (SXR emission) toroidally coupled modes in OH discharge #13532*

conditioning (due to a new oil-free vacuum pump) and plasma-wall interaction (due to installation of new graphite belt limiters) made possible to operate at currents in excess of 230 kA and high average densities in the target OH regime. The line average density ~(1.1-1.2)×10^{20} m^{-3} was achieved at the final stage of the discharge. No signatures of low m, n MHD modes activity were recorded. At such conditions the density was basically controlled externally by the inner-wall gas puff and the contribution of the walls could be neglected. Boronization was a part of vessel conditioning technology. Another important component of experimental scenario was the cycle in which the high density shot was alternated by several low density shots to prevent wall saturation by deuterium and minimize neutral gas wall recycling.

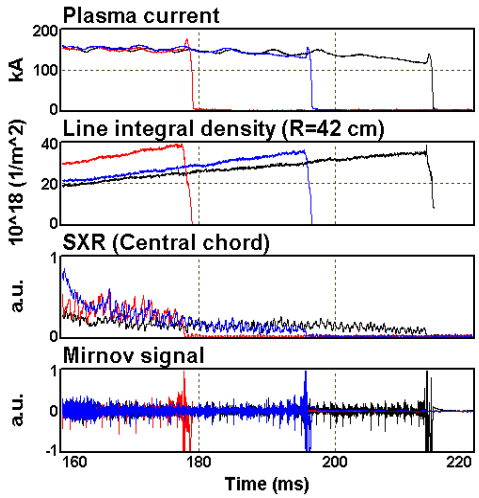

Fig.2 *Density limit approach at different gas puff rates: slow (shot #16159, black traces), middle (shot #16186, blue traces) and fast (shot #16173, red traces). The plasma breakdown is at 113 ms.*

The last series of high density experiments [9] were carried out at the toroidal magnetic field of 0.4 T and plasma currents of 150-250 kA. In contrast to our previous experiments, the plasma current degradation at high density was prevented by a feedback stabilization system. This system tries to keep constant current at higher density by increasing the loop voltage and OH power. The inner and outer wall gas puffing as well as their combination was used for the density control. The experiments have demonstrated that gas puff efficiency does not depend on the valve position. The simultaneous operating of two valves does not increase efficiency also, and density rise rate is only determined by the total gas flow. Fig.2 shows the limit density approach at three different gas puff rates: from minimal (shot #16159) to maximum one (shot #16173). It is seen from the figure that the density reaches approximately the same value, but at different time. High density shots are characterized by the low MHD activity level that is confirmed by Mirnov signals, shown in the figure. Generally the only observed MHD instability was saw-tooth oscillations, registered by the SXR camera. The highest amplitude of the saw-tooth oscillations was in the shots with faster density increase. It may be explained by sharper electron temperature profile in these discharges, arising due to the peripheral cooling with intensive gas flow, and hence sharper current density profile. This assumption is supported by electron temperature profiles $T_e(r)$ measured by means of Thomson scattering and safety factor $q(r)$ profiles reconstructed with equilibrium code EFIT. However, the saw-tooth oscillations seemed not to restrict the density rise, as their magnitude did not affect the value of the Greenwald parameter, $\langle n \rangle / n_{GW}$. On exceeding this limit, a discharge is terminated by disruption according with radiation collapse scenario: fast peripheral cooling, impurity radiation rise, recorded by a bolometer and OIII and CIII lines (see Fig.3), and, at last, magnetic reconnection leading to disruption. The Greenwald density limit (inside the measurement errors of 10%) was achieved in OH regime. Experiments showed that minimization of the impurity content led to 1/1 mode suppression and increase OH absolute average density limit up to values more than 1×10^{20} m^{-3}.

Attempts to exceed the Greenwald limit were carried out at auxiliary heating by means of the neutral beam co-injection with energy from 22 to 28 keV and power of 300-500 kW. The implementation of NBI has allowed us to extend the density limit in the absolute value due to operation at higher plasma currents – the points in Hugill diagram corresponding to NBI shots

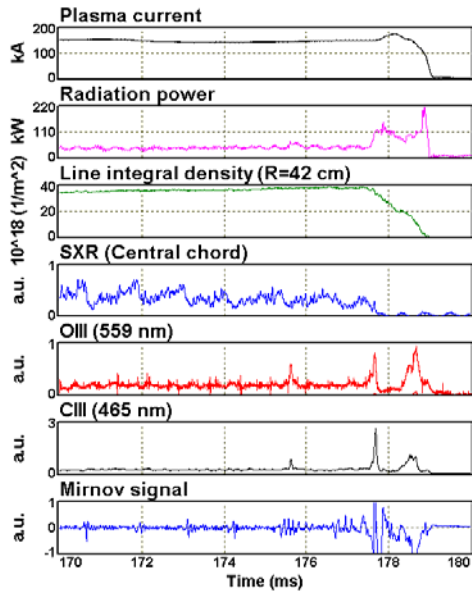

Fig.3 *Waveforms demonstrating radiation collapse at density limit in OH shot #16173*

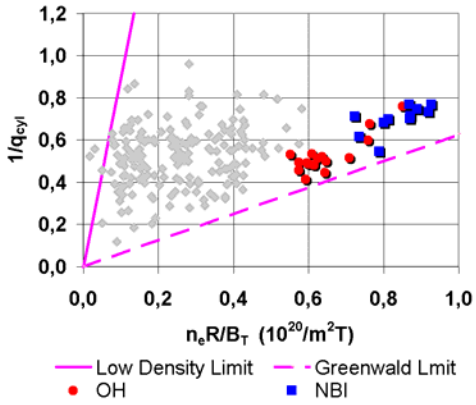

Fig.4 *Hugill diagram for Globus-M shots. Colored points correspond to the last year high density experiments*

(in Fig.4) are placed righter than the points corresponding to OH shots (blue rectangles versus red circles). But NBI has not increased essentially the Greenwald parameter. The following explanation may be done. The easier way to approach the Greenwald limit is operation at lower plasma currents and, hence, higher *q(a)*. The Greenwald parameter ~1 in OH shots has been achieved at the plasma currents 130-150 kA. But poor confinement of energetic ions at such currents makes NBI ineffective. Increase of the plasma current up to 200-250 kA leads to weaker MHD stability due to lower *q(a)*, and these OH shots suffer from internal reconnection events (IRE). Injection of the NB stabilizes IRE (mainly due to current profile modification) and permits achievement of higher plasma density, due to additional power, required for ionization and heating of the neutral gas incoming from the gas puffing. As a result, the density achieved at NBI was by 20% higher as compared with OH shots at the same other conditions. Such modest enhancement of the limit density corresponds to the scaling obtained on ASDEX [10], which defines that limit density $n_{lim} \sim P_{in}^{0.25\text{-}0.4}$, where P_{in} – input power. The input power in OH regime (about *400-500 kW*) is doubled at NBI, which leads to 20-30% increase of the density limit in accordance with the scaling. Further increase of the limit is possible at higher NBI power that can be realized with a new more powerful ion source, which is under preparation now.

3. Neutral Beam Heating Experiments

Experiments with the neutral beam injection were continued during the last period. Ion sources used allow overlapping the power range from ~0.3 to ~1.0 MW with energy of the injected particles varied from 20 to 30 keV. Initially we compared the efficiency of plasma heating by means of hydrogen and deuterium beams with identical energy and power during one experimental day [11]. The effect of ion heating appeared to be approximately the same in both experiments (see Fig.5). Some minor difference was in agreement with ASTRA code simulation and was caused by the difference in the beam particle velocity at the same energy. Only the deuterium beam was

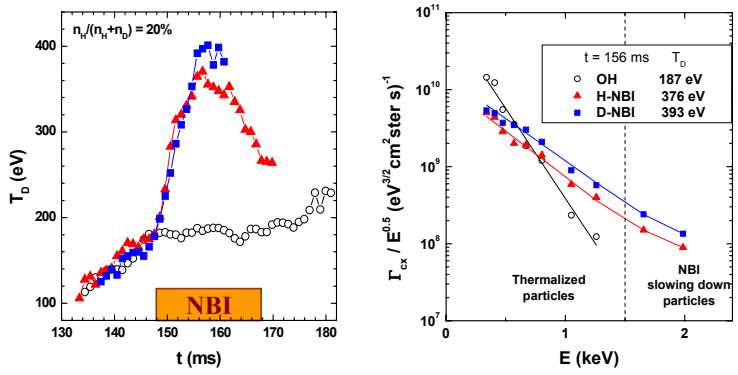

Fig.5 *Comparison of hydrogen and deuterium beam injection. Ion temperature time evolution (left), charge-exchange deuterium energy spectra (right). P_{NB} = 0.6 MW, E_{NB} = 30 keV, Ip = 0.15-0.16 MA.*

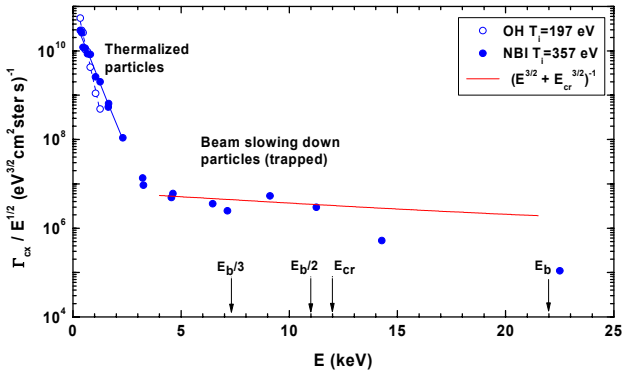

Fig.6 *Energy spectra of charge-exchange neutrals emitted from plasma during NBI. E_{NB} = 22 keV.*

used in further experiments. Investigation of the beam power absorption was carried out in the range of the average plasma densities (1-3)×10^{19} m^{-3} and currents 0.18-0.2 MA, where the ion heating is more pronounced [11]. The energy of the injected particles varied from 20 to 30 keV. The experiments revealed the beam absorption efficiency increases with the plasma density increase. On the other hand the maximum effect of ion heating was achieved for the beam energy of 22–25 keV in accordance with numerical simulation. The spectra of CX atoms in the energy range 0.2–22.5 keV are shown in Fig. 6. At the thermal energies (<2 keV) the spectra for both NBI heated shot and reference OH shot are shown. At the suprathermal energies (above 4 keV) a slowing down spectrum of beam deuterons is shown. It is significant that the CX fluxes were measured in the perpendicular direction, while the beam was injected tangentially. Therefore the slowing down spectrum represents the beam particles, scattered at significant angles (~90 deg). So called critical energy [12], proportional to the electron temperature is E_{cr}~12 keV for given discharge parameters. Above this energy electron drag predominates and the pitch angle scattering is not sufficient. As the result, the intensity of CX flux in the energy range 12-22.5 keV was lower. Below E_{cr} the pitch angle scattering becomes appreciable due to collisions with plasma ions. This explains the higher level of CX flux observed in the energy range of 0–12 keV. Also the slowing down spectrum below E_{cr} shows good correlation with the general dependence $E^{1/2}\times(E^{3/2}+E_{cr}^{3/2})^{-1}$, obtained on the assumption of negligible particle losses [13]. This indicates that the process of beam ion slowing down is well described by classical Coulomb scattering theory and that the particle losses at least in the energy range below E_{cr} are insignificant.

The investigation of ion heating as a function of the plasma density in wide range is a challenging task. Different control and diagnostics problems complicated such experiments. Previously ion temperature degradation was often observed after maximum value achieved during action of NB pulse. Due to the improved equilibrium control we obtained a possibility to operate without ion temperature degradation during the whole NBI pulse [14]. The dependence of the ion heating efficiency on electron density was investigated in such improved conditions with NB of 25 keV energy and beam power of ~0.6 MW. Fig. 7 demonstrates increase of the ion temperature during NBI pulse in shots with line averaged plasma density varied in a wide range (1-6)×10^{19} m^{-3}. One can see that maximum ion temperature reaches at low density below 2×$10^{19}$$m^{-3}$ (black curve in Fig.7a). The ion temperature increase reduces with density rise (red and green curves) and vanishes at the densities exceeding 5×$10^{19}$$m^{-3}$ (blue curve). In contrast, the electron temperature measured by Thomson scattering does not increase during NBI pulse at low density and demonstrates only a weak rise tendency at the densities higher 5×$10^{19}$$m^{-3}$. Such

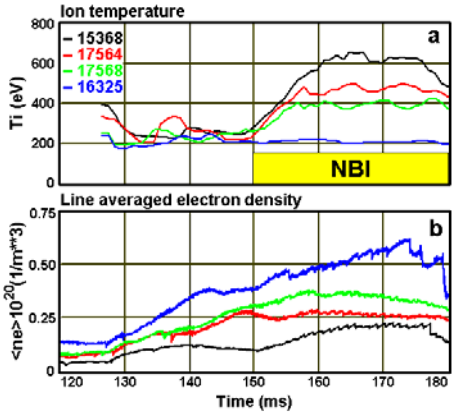

Fig.7 *Behavior of the central ion temperature T_i (0) and line averaged electron density <n_e> at NBI heating*

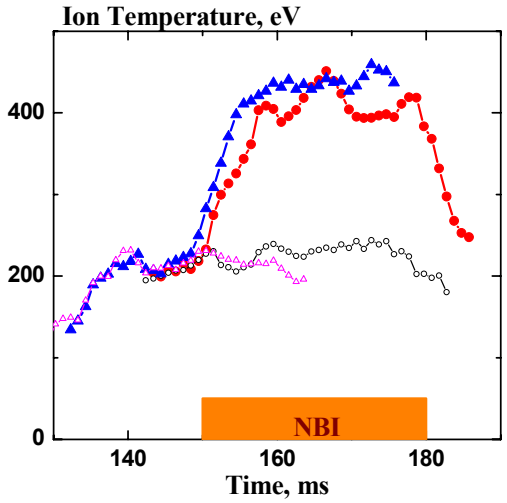

Fig.8 *Ion temperature evolution in shots #16776 (blue, Rs=30cm) and #17023 (red, Rs=33cm)*
P_{NB} *= 0.35 MW,* E_{NB} *= 23 keV,*
I_p*= 0.2 MA,* n_e *= (2-3)×*$10^{19}m^{-3}$

behavior is in a agreement with ASTRA code modeling, predicting that the power absorbed by electrons at NBI became comparable with OH power only at the densities $> 6\times10^{19}m^{-3}$ [15]. Features of "electron heating" were demonstrated in high density regime with line average densities in excess of $6\times10^{19}m^{-3}$ [8]. At the high plasma current 230-250 kA and beam parameters (*~30 keV*, *~0.6 MW*) constant density rise with some electron temperature degradation led to electron component stored energy increase. At slightly changed experimental conditions and lower plasma currents 170-190 kA, when plasma current stabilization was on, the electron temperature rise was recorded during NBI for the first time in Globus-M. Density profile seems to peak in this regime.

Dependence of the beam impact radius on plasma heating was investigated in the experiment described in [14]. Usually we inject the beam tangentially with the impact radius of 30 cm. This injection line was chosen in accordance with preliminary simulations by ASTRA code. In recent experiments the injection line was moved by 3-4 cm towards the machine axis from its initial position (from R_s*=30 cm* to R_s*=33-34 cm*). The time evolution of the ion temperature for the cases of regular and shifted impact radii is shown in Fig. 8. For both shots the ion temperature had similar behavior and reached approximately the same steady state values.

4. Fundamental IC harmonic hydrogen minority heating

The efficiency of single-pass absorption of FMS waves in resonance layers is not high at conditions of Globus-M. The width of cut-off barriers is also not so high. This leads to principal discrepancy between the features of wave excitation in conventual tokamaks and spherical tokamaks. In conventual tokamak the waves excitation is much more similar to the radiation in free space, whereas in spherical one wave propagation similar to a resonator kind, when the whole tokamak vessel plays the role of a multimode resonator of low quality. Another specific feature of Globus-M experiments is capability of varying of hydrogen "minority" concentration in very wide range $C_H = n_H/(n_H+n_D) = 10 - 50\%$ and even more, what can change the efficiency of wave energy absorption in the vicinity of cyclotron harmonics.

The ICRH simulations and experiments were continued with the emphasis on parametric dependence of heating efficiency. The wave absorption efficiency was examined by using a 1D code which was elaborated at Ioffe institute [16]. The code describes the propagation of fast magnetosonic (FMS) waves with allowance for cyclotron absorption, Landau damping and magnetic pumping in FLR approximation. Calculations were performed in cylindrical geometry, which corresponded to a tokamak with an infinite elongation. The plasma in this model is confined between two vertical coaxial cylindrical surfaces. The radial dependences of all parameters were taken as they are in the equatorial plane of the real Globus-M tokamak. Code description and simulations results discussion is given in [2]. It should be reminded that the single-loop antenna installed in the chamber port and used for FMS wave excitation [17] has a hundred times smaller dimension than the wave length. This fact leads to a very broad wave

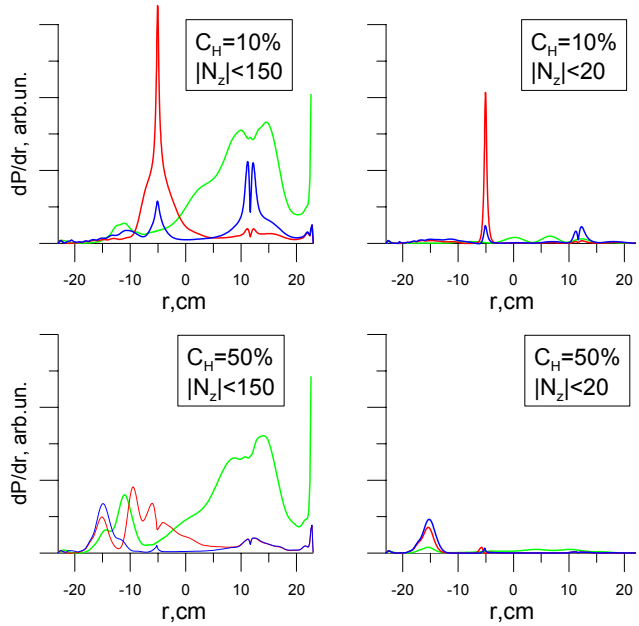

Fig.9 *Profiles of RF energy absorption in case of single-loop antenna. Left - $|N_z|\leq 150$, right - $|N_z|\leq 20$*

spectrum excited by the antenna (up to $|N_z|\approx 150$). To compare the role of different spectral components on the wave's absorption two different cases were compared. The Fig.9 demonstrates profiles of RF energy absorption by various plasma species calculated for the case of single-loop antenna. The RF power fraction absorbed is plotted as the function of Globus-M minor radius, with *r=0* corresponding to vessel geometrical axis. The profiles presented in the left column are calculated for the whole spectrum ($|N_z|\leq 150$). In the right column the absorption of the narrow part of the spectrum ($|N_z|\leq 20$) are shown. Green lines show the absorption by electrons (Landau damping and magnetic pumping mechanism), red lines – by hydrogen (cyclotron and Bernstein wave absorption) and blue lines – by deuterium. Profiles of RF energy absorption by ions are determined by localization of resonance zones. The energy absorption occurring on the left from ion-ion hybrid resonance position (at $r \approx -10 - -15$ *cm*) is accounted for by Bernstein wave born in this resonance. The energy release at $r \approx 10 - 15$ *cm* (in the third harmonic vicinity) can be associated with absorption of weak Bernstein wave excited directly by the antenna. The absorption by ions around fundamental hydrogen resonance ($r \approx -5$ *cm*) is classical when $|N_z|\leq 20$, i.e. vanishing with C_H increase. Contrary in the case $|N_z|\leq 150$ rather large absorption is observed even at C_H=50%. Simulations show that the absorption around the fundamental cyclotron resonance for hydrogen at high concentration of C_H should be connected with short wave part of the spectrum excited by the single-loop antenna.

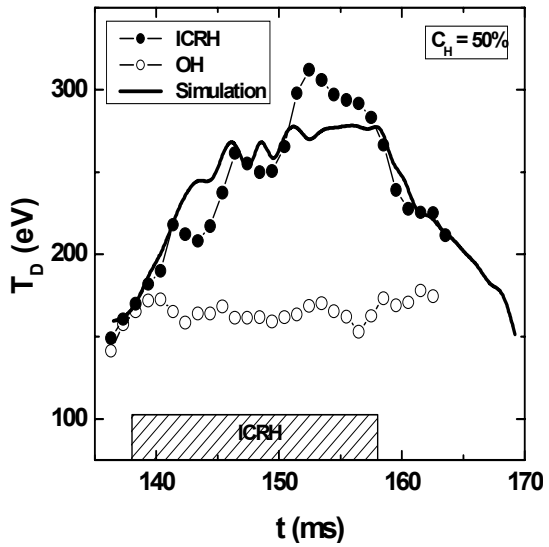

Fig.10 *Comparison of ion temperature dynamics during ICR heating in Shot #6736 with ASTRA simulation.*

The increase of ion temperature by a factor of 2-2.5 during RF power launch with maximum power 200kW in the target OH plasma of Globus-M were recorded during experimental sessions of 2005-2006. Experiments were made in the range of parameters: $B_{t0} = 0.4$ *T*, $I_p = 190 - 210$ *kA*, $f=7.5–9$ *MHz*, maximum absorbed RF power, $P_{inp}=120$ *kW*. Central plasma density was $(2\text{-}5)\times 10^{19} m^{-3}$. An energy exchange between plasma components (protons, deuterons and electrons) was simulated by the ASTRA 1.5-D numerical transport code. Analysis was performed for the plasma shot with RF heating when the 2nd cyclotron hydrogen harmonic resonance was present at plasma periphery, which made heating less effective. ITER-89P L-mode scaling [18] for the electron and neo-classical Chang-Hinton scaling [19] for ion heat diffusivities were

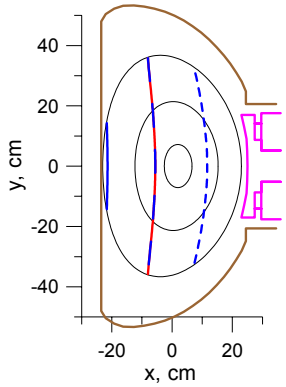

Fig.11 *Different resonances in Globus-M cross-section for 0.4T. FMS wave 7.5MHz is exited by single loop antenna, shown at the right by pink. From left-to-right:* $1\omega_{ID}$, $1\omega_{IH}$ *coinciding with* $2\omega_{ID}$, $3\omega_{ID}$.

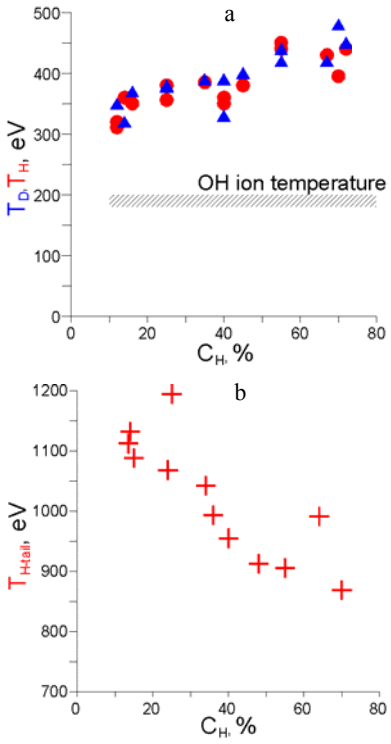

Fig.12 *(a) – Dependence of proton (red circles) and deuteron (blue triangles) temperatures on light "minority" (hydrogen) concentration in deuterium plasma during ICRH fundamental harmonic heating. (b) – Dependence of hydrogen tail "temperature" (red crosses) on light "minority" (hydrogen) concentration in deuterium plasma during ICRH fundamental harmonic heating*

assumed. The loop voltage was used as a fitting parameter to the experimental data. The satisfactory agreement between simulated ion temperature waveform and experimentally measured ones as well as the other parameters (current, voltage, power balance, etc.) was obtained at ion heat diffusivity value $\chi_i \approx 0.7\chi_i(neo)$. The comparison of simulated and experimental data is given at Fig. 10 [2].

Unlike good ion heating, reliable electron heating was not observed in these experiments, probably because the RF power absorbed by electrons (about 100 kW by RF code evaluation) is much less than the ohmic heating power (about 500 kW). The ASTRA simulation confirmed weak RF heating influence on electron temperature.

Last year experiments were performed to clarify the role of different parameters on heating efficiency. To minimize the simultaneous influence of different heating mechanisms we tried to limit the number of resonance layers placed inside plasma cross-section. For this purpose the RF generator and antennae chain was tuned to the operating frequency of 7.5 MHz. The resonances location inside the Globus-M vessel in the case of toroidal field, B_0 = 0.4 T, is shown on Fig. 11. Solid blue line presents the position of the fundamental resonance for deuterium, red dashed line presents the same resonance for hydrogen (and the second cyclotron harmonic for deuterium by blue dashed line), and short dashed blue line shows the position of the third harmonic of deuterium. The ion-ion hybrid resonance (not shown on Fig.11) shifts from the fundamental resonance for hydrogen to the deuterium one with increase of hydrogen/deuterium ratio. Important, that in such a conditions the 2nd harmonic of hydrogen, which is placed in front of antennae for higher frequencies is absent in plasma volume now. In regimes when the absence of 2nd hydrogen harmonic was guaranteed, the investigation of ion heating in dependence on hydrogen concentration C_H was performed. The ion temperature behavior was observed by a 12-channel NPA, which measured simultaneously hydrogen and deuterium fluxes and relative concentration of ion components. Two gas pulse valves were used for independent control of hydrogen and deuterium concentration keeping plasma density unchanged. Fig. 12 (a) demonstrates behavior of proton and deuteron temperatures during RF ICR fundamental harmonic light "minority" heating on the hydrogen concentration in very wide range. One can see from Fig. 12 (a) that ion heating improves when C_H is increasing from 12% to 75% in deuterium plasma. For comparison OH ion temperature range (180-200 eV) is shown by dashed area. Fig. 12(b) shows that at the same time

the effective hydrogen "tail" temperature (measured in the energy range 1.7 – 4 keV) decreased. Significant is that the ratio of the tail proton concentration to the thermal proton concentration drops sharply with increase of C_H (see the Table). It does mean that the total quantity of fast proton population in the plasma remained approximately the same in the course of experiment.

$C_H = n_H/(n_H + n_D)$	15%	25%	35%	50%	60%	70%
$\eta = N_{tail}/N_{therm}$	15,7	11,4%	11,5%	7%	4,8%	3,5%

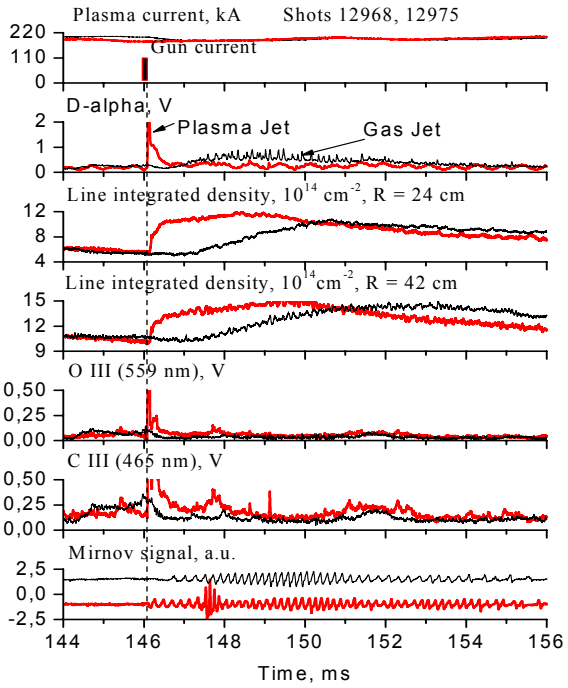

Fig.13 *Waveforms of plasma discharge parameters in Globus-M with gas jet (black lines) and plasma jet (red lines) injection*

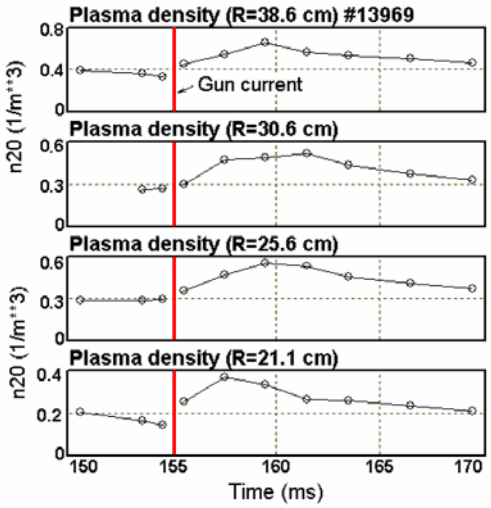

Fig.14 *Time and space resolved density variation before and after the injection of the plasma jet (measured by multi-pulse Thomson scattering diagnostics). The geometric axis of the column is at R=33 cm. Rather deep jet penetration into the plasma is evident.*

5. Plasma fuelling with coaxial plasma gun

Experiments on plasma jets injection into the Globus-M with a double-stage plasma gun were continued. To remind results which were published in different journals in 2005 – 2006, referred in introduction we summarize main of them below.

The hydrogen jet was injected into Globus-M in OH deuterium plasma during current plateau phase from the equatorial plane, along the major radius from the low field side. The jet speed was up to 110 km/s. The jet density near the gun edge reached 2×10^{22} m^{-3}. Typical waveforms of plasma parameters at full plasma current with plasma jet injection and for comparison with lower speed (~2 km/s) gas jet injection are shown in Fig.13. The distance between the plasma gun output and plasma was ~ 0.5 m, magnetic field at the center of the vessel was 0.4 T. One can see that time constant of density increase with plasma jet injection is much smaller, than with gas jet (gas jet pulse coincides in time with plasma jet).

To verify whether the density is increasing over the whole plasma column cross section, or it is the edge effect, the laser scattering measurements were made with ultimate temporal resolution. Time interval between successive laser shots was decreased down to 1 ms. Fig. 14 demonstrates the density temporal variation at different spatial points of major radius in Globus-M discharge before and during plasma jet injection. The time of injection is defined by red line.

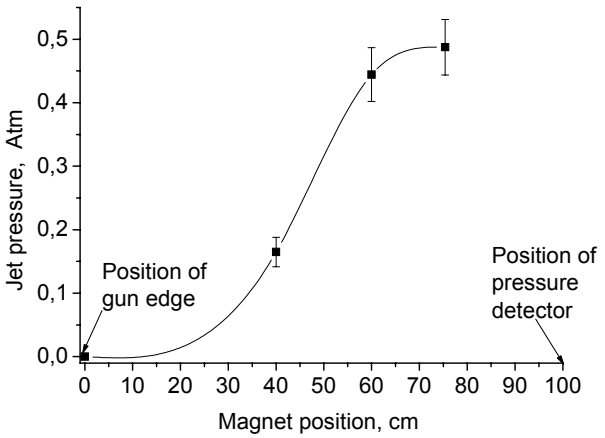

Fig.15 *Plasma jet pressure plotted vs distance between the DC magnet, B=0.3T and the plasma gun edge. Initial jet velocity is 75 km/s.*

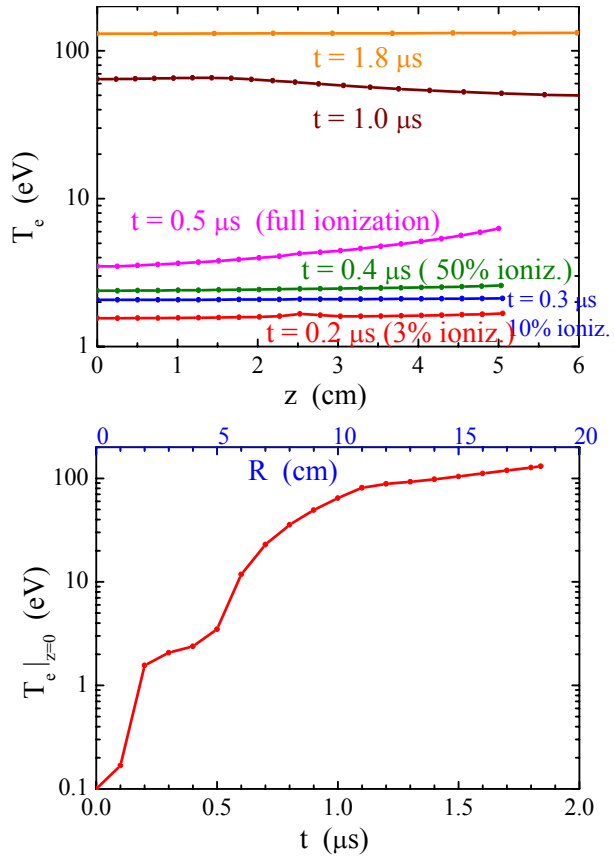

Fig.16 *Evolution of the jet temperature. (a) profiles along the magnetic field; (b): equatorial plane (z=0) temperature versus time.*

It was unclear how the jet could penetrate through the magnetic field, surrounding the plasma, because specific kinetic energy of the jet was insufficient to overcome the magnetic field pressure. The measurements with DC magnet of 0.3 T induction, performed at special experimental stand equipped with necessary jet diagnostics, resolved this problem. Fig.15 demonstrates the signal of the pressure gauge irradiated by the plasma gun from the distance of 1.0 m passed between the magnet poles. The signal varies as the magnet is moved from the gun towards gauge from zero level to full pressure (~0.5 Atm). The jet specific kinetic energy at the velocity of 75 km/s is less than magnetic pressure of 0.3 T field. Time-of-flight recombination of dense cold (1 eV) plasma jet into the jet of neutrals with the same density and velocity makes the jet insensitive to the magnetic field.

The penetration of jet into the core plasma requires more sophisticated theoretical consideration. For the jet penetration modeling the approach described in [20] was used. The heating, expansion and ionization of the jet penetrating towards the tokamak center are calculated for the typical density and temperature profiles. It is found that the initially neutral jet is getting ionized within $\tau_i = 0.5\ \mu s$, i.e. penetrates up to 5 cm assuming constant velocity. Temporal evolution of jet temperature is shown in Fig.16. Note that the timescale of full ionization in the Globus-M is of the same order as in experiments on Tore-Supra and ASDEX-Upgrade [21, 22], where the jet with similar parameters was accelerated by pressure gradient through Laval nozzle. The penetration of ionized jet in the injection direction is provided by polarization electric field $\vec{E}_0 = \left[\vec{B} \times \vec{V}_0\right] / B^2$ and $\vec{E} \times \vec{B}$ drift. However, this polarization and jet velocity $\vec{V}_{jet}$ respectively reduce due to two deceleration processes. First are currents in the Alfven wave emitted into the ambient plasma (the effect of so-called Alfven conductivity). The second is vertical ∇B-induced currents. Due to emission of Alfven wave the ionized jet decelerates exponentially and penetrates inside Globus-M plasma up to $V_0 \tau_\Sigma \approx 8$ cm, where $\tau_\Sigma \approx 0.8\ \mu s$ - characterizing deceleration time. Consequently, in the Globus-M deep penetration up to

$V_0(\tau_i + \tau_\Sigma) \approx 12$ cm $\approx$ a/2 is possible, while on ASDEX-Upgrade $V_0\tau_\Sigma \approx 1.5$ mm $<< a$, and jet practically could not cross the separatrix. Note that τ_Σ is inversely proportional to the square root of ambient plasma density and proportional to the jet density, therefore for higher ambient plasma densities and lower jet density the penetration depth would be smaller. The second process accelerates the jet towards the low field side. The ∇B - induced current leads to acceleration towards the low field side, however, this current in the jet expanding along the magnetic field vanishes at timescale $R\sqrt{m_i/(T_e + T_i)}$ due to rotational transform, which leads to a displacement of the same order [23]. As both processes are going simultaneously consideration is more complex, but one can expect within the computational model that significant part of injected particles should be deposited inside the separatrix, mainly at the plasma periphery when the jet was injected from the low field side. This does not contradict experimental observations. If one could imagine jet injection from high field side the depth of injection into the plasma column will increase significantly. Important result of the simulations is the weak sensibility of particle deposition to the initial ionization degree of the jet. It is explained by rather fast ionization, as the ionization time is smaller that any other characterizing time in the problem.

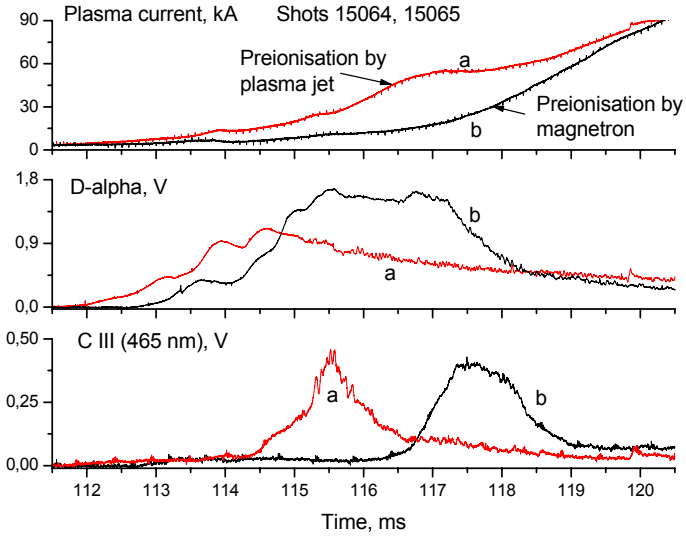

Fig.17 *Time history of some plasma parameters in Globus-M at different discharge initiation conditions; a-with plasma gun; b-with gas prefill and UHF preionozation.*

The study of discharge initialization by the plasma gun was continued in the last series of experiments. The plasma jet was injected at the time moment of maximum loop voltage when UHF preionozation and prefill of the vacuum vessel were off. Plasma source was placed at the equatorial plane on the distance of 0.5 m from plasma. Initial plasma velocity reached 100 km/s; number of injected particles was comparable with total number of the particles in tokamak (5×10^{18} – 1×10^{19}). The traces of plasma discharge, initialized by means of plasma jet are shown in Fig. 17. One could see that plasma current ramps up faster with the plasma gun initiation, than with traditional method. It is also seen that maximum of the spectral line intensities (D-alpha and CIII) are shifted to the beginning of the discharge. Higher plasma current and earlier spectral lines excitation may confirm more intensive plasma heating at the initial stage of the discharge.

6. Summary

New results were obtained during the reported period practically at all main direction of Globus-M tokamak research program. High densities near the Greenwald limit are obtained both in OH and NBI heating regimes. Important that the value of average density, obtained in low field of 0.4 T reaches $(1.1\text{-}1.2)\times10^{20}$m^{-3} at gas puff supply. NBI fundamental processes were studied. Experiments shown that slowing down of beam ions is well described by classical Coulomb scattering theory and the particle losses with energies below E_{cr} are

insignificant. Different heating regimes were obtained dependent on target plasma density. Regimes with overheated ions are achieved at densities below $2.5\times10^{19}m^{-3}$, heating of electrons is observed at densities higher $(5\text{-}6)\times10^{19}m^{-3}$. The ICR heating study at the fundamental harmonic range were continued on Globus-M tokamak both in theory and experimental directions to make clear and self consistent the picture of RF heating in conditions of spherical tokamak. Fundamental harmonic ICR heating efficiency improvement with hydrogen minority concentration increase in the wide range of 10 – 70% was recorded experimentally and confirmed by simulations. The negative role of second harmonic hydrogen resonance positioning was outlined in the experiments. The reliability of the plasma gun as the source for plasma feeding and the instrument for the discharge initialization was confirmed. Numerical simulations of plasma jet interaction with core tokamak plasma were started, giving first results in tolerable agreement with experiments.

This work is supported by the Russian Academy of Science, Ministry of Science and Education, Federal Atomic Energy Agency, IAEA Research Contract No 12408, RFBR grants ## 04-02-17606, 05-02-17763, 05-02-17773, 05-08-18044, 06-02-08142, 06-02-08186, 06-02-16709, 06-02-16189.

References

1. Gusev V.K., et al., *Tech. Phys.* **44** (1999) 1054
2. O.N. Shcherbinin, et al., *Nuclear Fusion* **46** (2006) S592-S577
3. Abramova K.B., et al, *Plasma Physics Reports* **31** (2005) 1
4. Voronin A.V., et al., *Nuclear Fusion* **45** (2005)1039–1045
5. A.V. Voronin, et al., *Nucleonica* 2006 **51** (1), p. 85 – 92
6. Yu.V. Petrov et al., *Proc. 3d IAEA TM on ST, St.Petersburg* 2005, CDROM, OV-4
7. V.K. Gusev et al., *Proc. 31st EPS Plasma Phys. Conf. London* 2004, ECA, **28G** P4-158
8. V.K. Gusev, et al., *Nuclear Fusion* **46** (2006) S584-S591
9. Yu.V. Petrov et al., *Proc. 33rd EPS Plasma Phys. Conf., Roma*, 2006, ECA **30**, P4-103
10. Stäbler A. et al, *Nuclear Fusion* **32** (1992) 1557
11. V.B. Minaev et al., *Proc. 32nd EPS Plasma Phys. Conf. Tarragona*, 2005, ECA **29C**, P-1.103
12. W.W. Heidbrink, G.J. Sadler, Nuclear Fusion, **34** (1994) 535
13. Chernychev F.V., et al., *Plasma Phys. Contr. Fusion* **41** (1999) pp. 1291-1301
14. V.B. Minaev et al. *Proc. 33d EPS Conf. on Plasma Phys. Roma*, 2006, ECA **30**, P-4.104
15. L.G. Askinazi *et al., Plasma* Devices and Operation, 11 (2003) No.3, 211-21810
16. Irzak, M.A., et al., *Plasma Physics Reports* **25**(8) (1999) 659
17. Gusev, V.K., et al, *Tech. Phys. Lett.* **30**(8) (2004) 690
18. Yushmanov, P.N., et al., *Nuclear Fusion* **30**(10) (1990) 1999
19. Chang, C.S., Hinton, F.L., *Phys. Fluids* **29** (1986) 3314
20. V. Rozhansky et al. *Nuclear Fusion* **46** (2006) 367-382
21. J. Bucalossi et al, *Proc. 29th EPS Conf. on Contr. Fusion, Montreaux*, 2002, ECA **26B**, O-2.07
22. P.T. Lang, et al. *Plasma Phys. Contr. Fusion* **47** (2005), 1495-1516
23. V. Rozhansky et al. *Plasma Phys. Contr. Fusion* **46** (2004) 575-591